Sizeable mixing between the coexisting normal and intruder structures of ^{96}Zr revealed through lifetime measurements

T. Beck [1,2,*] T. Stetz,[1] N. Gavrielov [3] N. Pietralla [1] V. Werner [1] K. Yanase [4,†] M. Boromiza [5] A. Coman [5] C. Costache [5] N. M. Florea,[5] I. Gheorghe [5] A. Ionescu [5] R. Lica [5] N. Mărginean,[5] R. Mărginean [5] H. Mayr [1] C. Mihai [5] R. E. Mihai [5] A. Mitu [5] C. R. Nita,[5] T. Otsuka [6] O. Papst [1] S. Pascu [5] C. Sotty,[5] L. Stan [5] S. Toma [5] Y. Tsunoda [6,7] A. Turturică [5] S. Ujeniuc [5] and J. Wiederhold [1]

[1]*Department of Physics, Institute for Nuclear Physics, Technische Universität Darmstadt, 64289 Darmstadt, Germany*

[2]*Instituut voor Kern- en Stralingsfysica, KU Leuven, B-3001 Leuven, Belgium*

[3]*Physics Department, Nuclear Research Center-Negev, P.O. Box 9001, Beer-Sheva, Israel*

[4]*RIKEN Nishina Center, RIKEN, 2-1 Hirosawa, Wako-shi, Saitama 351-0198, Japan*

[5]*Horia Hulubei National Institute for R&D in Physics and Nuclear Engineering, Strada Reactorului 30, POB MG6, RO-077125 Bucharest-Măgurele, Romania*

[6]*Center for Nuclear Study, University of Tokyo, 7-3-1 Hongo, Bunkyo-ku, Tokyo 113-0033, Japan*

[7]*Center for Computational Sciences, University of Tsukuba, 1-1-1 Tenno-dai, Tsukuba, Ibaraki 305-8577, Japan*

(Received 30 June 2026; accepted 20 October 2026; published 13 November 2026)

Lifetimes of excited states of the nucleus ^{96}Zr were studied with the Doppler-shift attenuation method following the ^{94}Zr(^{18}O, ^{16}O)^{96}Zr two-neutron transfer reaction. The obtained $B(E2; 2_2^+ \rightarrow 0_2^+)$ and $B(E2; 4_1^+ \rightarrow 2_2^+)$ transition strengths, amounting to 26(2) and 39(7) W.u., respectively, firmly attribute the 2_2^+ and 4_1^+ states to the collective intruder band built on top of the 0_2^+ state. The nature of this structure is discussed against predictions of the collective model using the Bohr Hamiltonian, the interacting boson model with configuration mixing, and the quasiparticle vacua shell model. The collective, interband $B(E2; 4_1^+ \rightarrow 2_1^+) = 11.2(8)$ W.u. transition strength, refuting the previously assumed purity of both structures, is reproduced in the calculations. The quasiparticle vacua shell model predicts, in agreement with a simple two-state model based on experimental $E2$ transition strengths, considerable mixing between the normal and intruder 2^+ states.

DOI: 10.1103/f171-t9xh

I. INTRODUCTION

The zirconium isotopic chain has historically played a pivotal role in the understanding of the emergence of collective behavior from the single-particle properties of individual nucleons. In their seminal work, Federman and Pittel attempted an explanation of nuclear deformation in the $A \approx 100$ mass region from the proton-neutron correlations between spin-orbit partners [1]. The monopole part of the tensor interaction has subsequently been identified as quintessential for these attractive proton-neutron interactions driving the evolution of nuclear structure [2–4]. While this behavior has traditionally been associated with the addition of nucleons, the influence of nucleon configurations within a single nucleus on the nuclear structure as a function of excitation energy has been highlighted more recently [5]. Following the interpretation of the rapid shape change found for zirconium isotopes near neutron number $N = 60$ in the context of this so-called type-II shell evolution by Togashi *et al.*, the study of zirconium isotopes experienced a renaissance in the past decade; e.g., Refs. [6–14].

The rapid quantum phase transition from spherical ground states for $^{90–98}$Zr to deformed ones for ^{100}Zr and heavier isotopes has in the past been described theoretically using, notably, the shell model and Hartree-Fock-Bogoliubov methods [1]. A compilation of further approaches is found in Ref. [15]. More recently, calculations using the Monte Carlo shell model [16,17] (MCSM) and in the interacting boson model with configuration mixing [18,19] (IBM-CM) have shifted the focus to excited-state (intruder) structures [5,20–23]. While both approaches are qualitatively in agreement for the ground-state structures with respect to excitation energies and $E2$ transition strengths, they show deviations for intruder configurations possibly rooted in the inclusion of more than two configurations in the MCSM calculations.

For ^{96}Zr, the influence of the $N = 56$ neutron subshell closure pushes the 2_1^+ state to 1750.497(15) keV [24], leaving the intruder 0_2^+ state at 1581.64(6) keV [24] as the first excited state. In the MCSM it is predicted to be of triaxial nature [5] in contrast to the IBM-CM calculations where it is characterized by a predominantly spherical, U(5)-like configuration [21]. Both approaches reproduce the single-particle nature of the

*Contact author: tobias.beck@kuleuven.be

†Present address: Department of Physics, Chiba Institute of Technology, 2-1-1 Shibazono, Narashino, Chiba, 275-0023, Japan.

Published by the American Physical Society under the terms of the Creative Commons Attribution 4.0 International license. Further distribution of this work must maintain attribution to the author(s) and the published article's title, journal citation, and DOI.

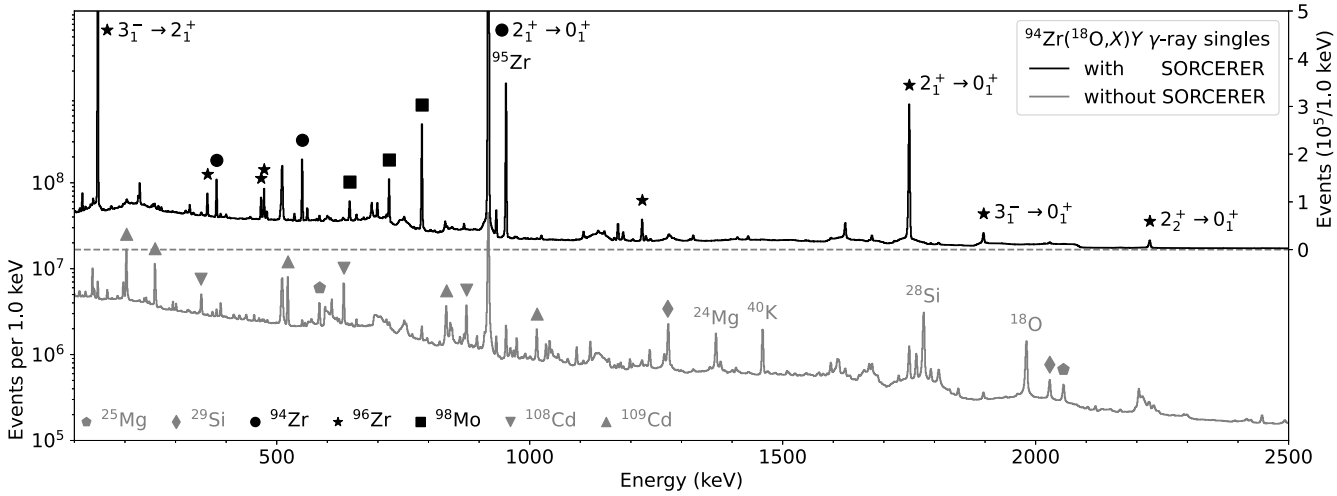


FIG. 1. Compton-suppressed γ-ray spectra of ROSPHERE with (black, top) and without (gray, bottom) a condition on the photodiodes of SORCERER. The former spectrum, using the linear scale on the right, shows the strong suppression of γ rays originating from nuclei created in fusion-evaporation reactions. Known γ-ray lines of the target ^{94}Zr as well as ^{96}Zr and ^{98}Mo produced in two-neutron and α-transfer reactions are marked by circles, asterisks, and squares, respectively.

transition between the 2_1^+ and ground states characterized by a small transition strength of $B(E2; 2_1^+ \rightarrow 0_1^+) = 2.3(3)$ W.u. [6]. The experimental value for the $E2$ transition strength of the corresponding transition between the intruder 2_2^+ and 0_2^+ states is about one order of magnitude larger; a value of 39(6) W.u. has recently been proposed [25]. The minuscule transition strength $B(E2; 2_2^+ \rightarrow 0_1^+) = 0.26(8)$ W.u. [6] connecting the normal (ground-state) and intruder configurations reveals their decoupled nature; a feature reflected by a small mixing between them in the calculated IBM-CM wave functions [23].

The characterization of the intruder configuration requires new precision data, especially for the $E2$ transition strengths between its members, to facilitate a comparison to theoretical models. A new calculation of ^{96}Zr with the quasiparticle vacua shell model [26,27] (QVSM) proposes values of 25.7 and 37.7 W.u. for the $2^+ \rightarrow 0^+$ and $4^+ \rightarrow 2^+$ $E2$ transitions in the intruder band, respectively, comparable to IBM-CM predictions of 28.8 and 43.5 W.u. [21]. In the literature, the 4_1^+ state at 2857.373(23) keV [24] is assigned intruder origin due to its large transition strength to the 2_2^+ state [28]. The latter has been calculated from the lifetime of $\tau(4_1^+) = 860^{+670}_{-260}$ fs determined with the Doppler-shift attenuation method (DSAM) after inelastic neutron scattering [29]. The upper relative uncertainty exceeding 75% leads to large fluctuations in the $B_{4/2} = B(E2; 4_1^+ \rightarrow 2_2^+)/B(E2; 2_2^+ \rightarrow 0_2^+)$ fingerprint, including the values $B_{4/2} = 2.0$ and 1.4 obtained for a spherical vibrator and a rigid rotor, respectively. For the ratio of excitation energies relative to the 0_2^+ state at 1581.64(6) keV [24], a value of $R_{4/2} = [E(4_1^+) - E(0_2^+)]/[E(2_2^+) - E(0_2^+)] = 1.98$ is found, which suggests vibrational character. In order to address these open questions on the nature of the intruder structure of ^{96}Zr, which were put forward in Ref. [28], its 4^+ and, if possible, 6^+ members have to be identified unambiguously and new precision lifetime measurements of the 2_2^+ and 4_1^+ states are needed.

II. EXPERIMENT AND RESULTS

In the present work, the ^{94}Zr(^{18}O, ^{16}O)^{96}Zr two-neutron transfer reaction was used to populate excited states of ^{96}Zr. The incident beam of ^{18}O ions was accelerated by the 9 MV FN Pelletron tandem accelerator [30] at the Horia Hulubei National Institute of Physics and Nuclear Engineering (IFIN-HH) in Bucharest-Măgurele, Romania, to 49 MeV; approximately 2 MeV below the Coulomb barrier of the projectile-target system. The thickness of the reaction target, enriched to 96.49(1)% in ^{94}Zr, was 7.22 mg/cm^2, resulting in a stopping of targetlike reaction products within the target to allow for the extraction of excited-state lifetimes with the Doppler-shift attenuation method [31,32]. Projectilelike reaction products, such as ^{16}O and ^{14}C after two-neutron and α transfer reactions, respectively, were detected with the SORCERER array [33,34] at backward angles with respect to the incident beam direction. The prototype of the array used in the present experiment consisted of seven silicon photodiodes in a circular arrangement, covering polar angles between approximately 122° and 164°. For detection of γ rays emitted by the excited reaction products, the target was placed in the center of the ROSPHERE array [35], consisting of 25 Compton-suppressed high-purity germanium (HPGe) detectors arranged in five rings at polar angles of 37°, 70°, 90°, 110°, and 143° with respect to the beam axis. The summed γ-ray spectrum of all detectors is shown in Fig. 1. Significant contributions to it stem from fusion-evaporation reactions of beam and target nuclei; in accordance with calculations using the computer code PACE4 [36–38] γ rays of ^{108,109}Cd are observed most prominently. Furthermore, a variety of lighter-mass nuclei such as ^{24,25}Mg or ^{28,29}Si are produced from reactions with the mounting structures of the target and SORCERER. Requiring a coincidence condition with the SORCERER array, these fusion-evaporation events are suppressed [33]. As evident from Fig. 2, the prototype of SORCERER used in the present experiment lacked the energy resolution to enable a selection of individual reaction

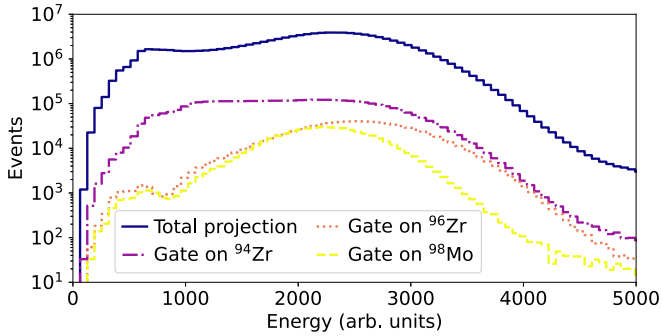


FIG. 2. Energies of reaction products in SORCERER from particle-γ correlations. The spectra for ^{94,96}Zr and ^{98}Mo are obtained from conditions in the γ-ray spectrum on the $2_1^+ \rightarrow 0_1^+$ transitions at 918.74(5) [39], 1750.42(2) [24], and 787.372(20) keV [40], respectively. Due to the broad, overlapping distributions, no clean reaction-channel selection based on the particle energy detected in SORCERER is feasible in the present work.

channels. As a consequence, the spectrum of Fig. 1 is dominated by transitions from excited states of ^{94}Zr populated in Coulomb excitation as well as ^{96}Zr and ^{98}Mo produced by two-neutron and α-transfer reactions, respectively. For the nucleus of interest, ^{96}Zr, 31 transitions between 20 nuclear levels have been observed and identified in the HPGe energy spectra. Their placement in the known level scheme [24] is facilitated through energies obtained from HPGe singles spectra and the analysis of $\gamma\gamma$ coincidence relationships. All observed γ-ray transitions are placed in the level scheme shown in Fig. 3 with arrow widths reflecting their relative intensities.

The determination of level lifetimes using DSAM requires precise information on the stopping process of ions inside the target material. The excited ^{96}Zr ions produced in the ^{94}Zr(^{18}O, ^{16}O)^{96}Zr reaction are moving in forward direction with respect to the beam axis with an initial velocity of $v/c \approx 0.03$ and are continuously slowed down within the target until at rest, resulting in an angular straggling of approximately 7.5°. The respective velocity distribution of this process is simulated with the program StopSim [41] using stopping powers calculated with SRIM [42]. The γ-ray lineshape analysis is performed individually for the five rings of ROSPHERE, i.e., the sets of detectors characterized by the same angle ϑ with respect to the beam axis, using the program APCAD [41]. The MIGRAD minimizer was used for all values presented in this work in combination with the MINOS algorithm to provide statistical uncertainties [43]. The calculated stopping powers, which are identified as the main sources of systematic uncertainties, were varied in the simulation process by ±5% and ±10% for the electronic and nuclear components, respectively. The energy dependency of the detector resolution was calibrated with a function of the form $f(E) = a + b\sqrt{E}$. A summary of the results obtained from the experimental data is given in Table I.

In the following, selected states are discussed individually. The two most intense γ rays of ^{96}Zr visible in the spectra shown in Fig. 1 originate from the $3_1^- \rightarrow 2_1^+$ and $2_1^+ \rightarrow 0_1^+$ transitions at 146.653(10) and 1750.42(2) keV [24], respectively. As evident from the level scheme shown in Fig. 3, the 2_1^+ state is populated by a multitude of higher-lying states; some of which without known lifetimes [24]. In the latter case, their lifetime is used as an additional free parameter in the DSAM analysis; ultimately yielding

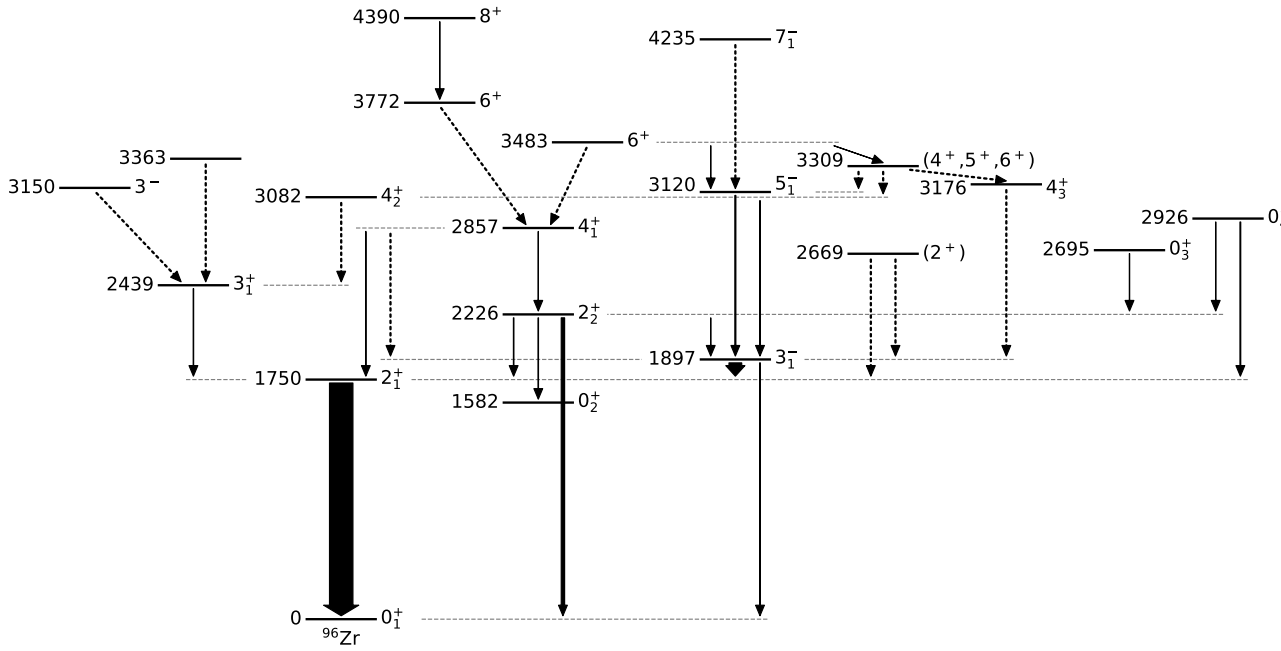


FIG. 3. Level scheme of ^{96}Zr as populated by the ^{94}Zr(^{18}O, ^{16}O)^{96}Zr reaction. Arrow widths reflect peak intensities and are taken relative to the $2_1^+ \rightarrow 0_1^+$ transition at 1750.42(2) keV [24]. Dotted arrows denote transitions only observed in $\gamma\gamma$-coincidence spectra. All energies, which are rounded to full keV, and quantum numbers are taken from Ref. [24].

TABLE I. Compilation of experimental data for the $2^+_{1,2}$ and $4^+_{1,2}$ states of ^{96}Zr. Angular-momentum and parity quantum numbers as well as excitation energies are taken from Ref. [24]. Transitions marked with an asterisk are used for the lineshape analysis (cf. Fig. 4). Reduced transition strengths for radiation character λL, which are calculated using branching ratios and, if available, multipole mixing ratios from Ref. [24], are given in $10^{-5}e^2\text{fm}^2$ for $E1$, μ_N^2 for $M1$, and W.u. for $E2$ with statistical and systematic uncertainties coming from the lifetime determination added in quadrature. Predictions of transition strengths obtained from the collective model using the Bohr Hamiltonian [44], the IBM-CM [21,22] with two choices for the mixing parameter ω, and the QVSM are given.

J^π	E_x (keV)	τ (ps)	J^π_f	E_γ (keV)	λL	$B(\lambda L, J^\pi \to J^\pi_f)$				
						Experiment	Coll. model	IBM-CM		QVSM
								$\omega = 0.02$ MeV	$\omega = 0.04$ MeV	
2^+_1	1750.497(15)	$0.63(5)_{\text{stat}}(7)_{\text{syst}}$	0^+_1	1750.42(2)*	$E2$	2.9(4)	5.23	2.57	2.90	1.57
			0^+_2		$E2$	[a]		1.49	3.91	10.1
2^+_2	2225.846(17)	$1.53(6)_{\text{stat}}(5)_{\text{syst}}$	0^+_1	2225.846(17)	$E2$	0.19(1)	0.39	0.001	0.001	0.08
			2^+_1	475.33(1)*	$M1$	0.098(6)[b]	0.071	0.024	0.058	0.097
			0^+_2	644.18(6)	$E2$	26(2)	26.0	28.8	26.0	25.7
			3^-_1	328.75(3)	$E1$	81(7)[c]				
4^+_1[i]	2857.373(23)	$1.22(4)_{\text{stat}}(6)_{\text{syst}}$	2^+_1	1106.88(2)*	$E2$	11.2(8)[e]	16.7	3.13	8.57	15.3
			3^-_1	960.9(2)	$E1$	6(2)				
			2^+_2	631.45(4)	$E2$	39(7)[f]	43.0	43.5	37.5	37.7
4^+_2[i]	3082.36(3)	$1.84(4)_{\text{stat}}(24)_{\text{syst}}$	3^-_1	1185.19(3)*	$E1$	15(2)[g]		[h]	[h]	
			4^+_1	224.8	$M1$	0.20(3)[j]		[h]	[h]	0.000018
			2^+_1	1331.8(2)	$E2$	0.30(5)		[h]	[h]	0.02
			3^+_1	643.9(2)	$M1$	0.006(1)[j]		[h]	[h]	
			2^+_2	856.6(2)	$E2$	1.7(4)		[h]	[h]	0.0

[a] Not observed [24].
[b] Calculated using $\delta = -0.09^{+0.01}_{-0.02}$ [24].
[c] Calculated using $\delta = -0.02(5)$ [24].
[d] Taken from Ref. [29].
[e] Calculated using $\delta = -0.03(3)$ [24].
[f] Calculated using $\delta = -0.02(8)$ [24].
[g] Calculated using $\delta = +0.02(3)$ [24].
[h] The 4^+_2 state lies outside the IBM-CM model space.
[i] The 4^+_1 state emerges as the 4^+_2 state in the QVSM calculations and vice versa.
[j] Assuming pure $M1$.

$\tau(2^+_1) = 0.63(5)_{\text{stat}}(7)_{\text{syst}}$ ps [cf. column (a) of Fig. 4]. This value is in agreement with 0.45(19) ps [24] obtained in an early Coulomb-excitation experiment using a ^{14}N beam but smaller than the lifetime of 0.82(10) ps found in Ref. [45] from DSAM after projectile Coulomb excitation, for which only feeding from the 3^-_1 state has been considered. A more recent result from DSAM after inelastic neutron scattering reported $\tau(2^+_1) = 770^{+180}_{-130}$ fs [46], in agreement with both, the present result and the value of Ref. [45].

The dominant feeding contribution to the 2^+_1 state is attributed to the 3^-_1 state at 1897.158(16) keV [24]. No lineshape is observed, indicating that its depopulating γ rays are predominantly emitted at rest, consistent with its comparatively long lifetime of 98(6) ps [24].

For the 2^+_2 state at 2225.846(17) keV, the known depopulating transitions to the $0^+_{1,2}$, 2^+_1, and 3^-_1 states have been observed with their determined branching ratios in perfect agreement with literature values [24]. An enhancement of the decay path to the 2^+_1 state, reported as 90(5)% and 70.1(14)% in Refs. [12] and [25], respectively, is not found. From the known $B(E2; 2^+_2 \to 0^+_1)$ transition strength, determined in inelastic electron scattering [6], a lifetime $\tau(2^+_2) = 1.1^{+0.5}_{-0.3}$ ps is deduced [28], significantly improving on the previously known upper limit of 10 ps [47]. In the present work, the lifetime of the 2^+_2 state is determined independently using its depopulating transitions to the 3^-_1 and 2^+_1 states at 328.75(3) and 475.33(1) keV [24], yielding consistent lifetimes of $1.2(2)_{\text{stat}}(5)_{\text{syst}}$ and $1.53(6)_{\text{stat}}(5)_{\text{syst}}$ ps, respectively. The latter value, which comes with greatly reduced uncertainty when compared to previous results, leads to transition strengths $B(E2; 2^+_2 \to 0^+_1) = 0.19(1)$ and $B(E2; 2^+_2 \to 0^+_2) = 26(2)$ W.u. with statistical and systematic uncertainties added in quadrature. These results are, however, smaller than the ones extracted from light ion-induced Coulomb excitation [25]. Reproduction of the latter would require an approximately 35% reduction in the lifetime of the 2^+_2 state, corresponding to more than six standard deviations.

Sizeable collectivity might be expected for the (2^+) state at 2668.82(4) keV [24] based on its known lifetime

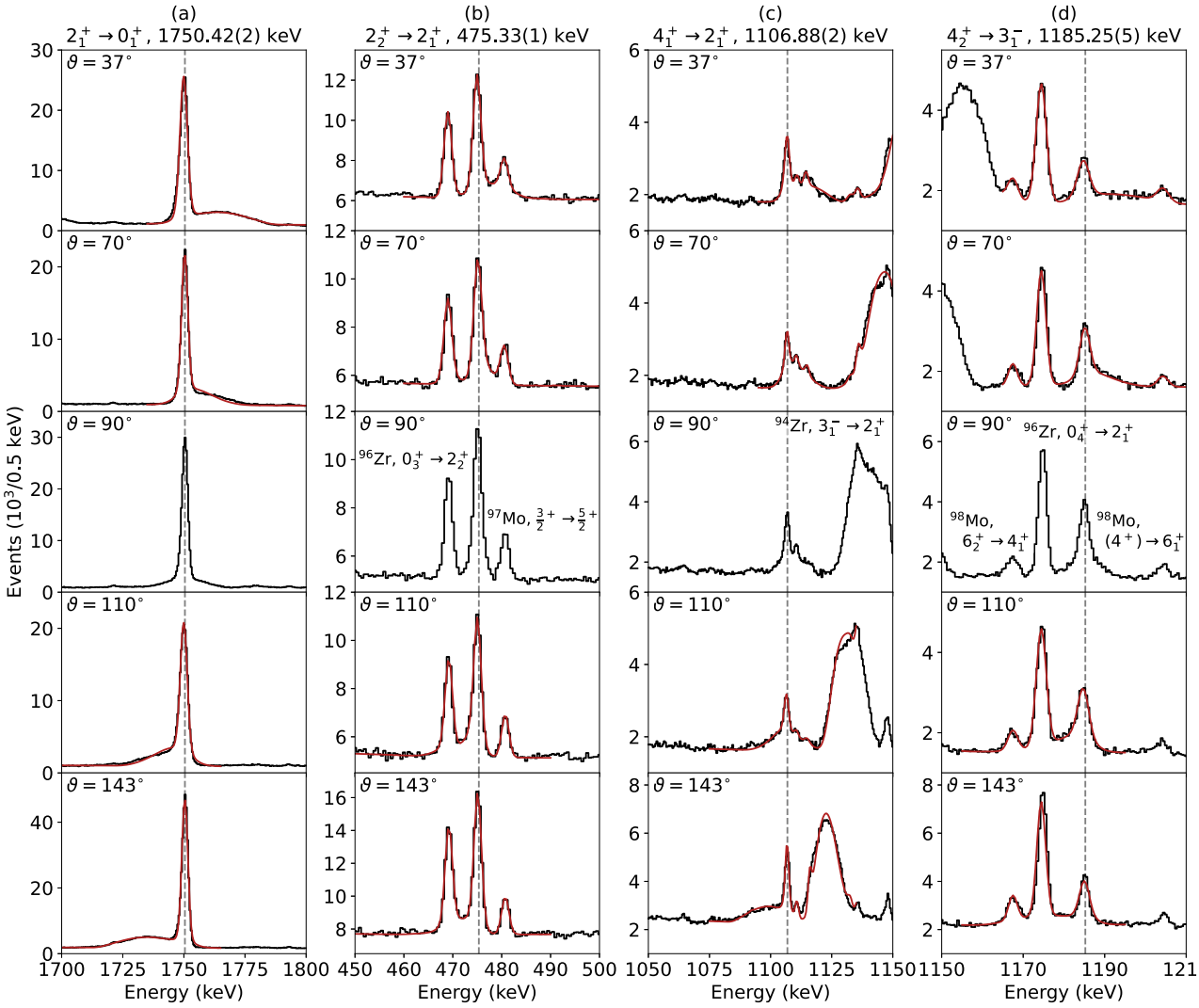


FIG. 4. Overview of particle-gated γ-ray spectra for transitions depopulating the $2^+_{1,2}$ and $4^+_{1,2}$ states (columns) at different detection angles of ROSPHERE (lines) together with adapted lineshapes from APCAD [41]. The ^{96}Zr transitions of interest are indicated by dashed vertical lines. For detection angles $\vartheta = 90°$, where no Doppler shifts are expected, the spectrum without the simulated lineshape is shown and major contaminant transitions are identified. The small peaks seen on the high-energy side of the 1106.88(2)-keV transition in column (c) are identified as the $7^-_1 \to 5^-_1$ and $5^-_1 \to 4^+_1$ transitions of ^{96}Zr and ^{98}Mo at 1114.6 [24] and 1110.77(7) keV [40], respectively. The lifetimes obtained for the individual rings are collected in Fig. 5.

of $0.35^{+0.46}_{-0.14}$ ps [29]. In the present work, however, a determination of the state's lifetime is not possible since its dominant decay branch to the 2^+_1 state is at virtually the same energy as the $2^+_1 \to 0^+_1$ transition of ^{94}Zr and the decay channels to the 2^+_2 and 3^-_1 states are too weak for a lineshape analysis.

In the literature, the first 4^+ state of ^{96}Zr is postulated at 2750(15) keV [24] based on results from particle spectroscopy following the ^{100}Mo(d, ^{6}Li)^{96}Zr reaction [48]. The authors confirmed a tentative $L = 4$ assignment for this state from Flynn *et al.* who studied inelastic triton scattering off ^{92,94,96}Zr [49]. In the latter work, which was the first one to report the observation of a level at 2750(15) keV, however, its affiliation with the level scheme of ^{96}Zr is dismissed, suspecting it to originate from a ^{90}Zr contaminant found in the scattering target. Indeed, a 3^- state of ^{90}Zr is known at an excitation energy of 2747.875(16) keV [50]. Neither in the present experiment, nor in any other recent one [12,24], evidence for the existence of a potential 4^+ state of ^{96}Zr at 2750(15) keV is found. Following the strategy put forward in Ref. [28], it is omitted in the ensuing discussion. Hence, the 4^+ state at 2857.373(23) keV [24] is, based on the discussion above, denoted the first 4^+ state of ^{96}Zr throughout this work. Since it is predominantly populated directly by the two-neutron transfer reaction, with feeding through the higher-lying $6^+_{2,3}$ states amounting to only about 2%, and a coincidence condition on the flight component of the $2^+_1 \to 0^+_1$ does not have sufficient statistics, the DSAM analysis can only be performed on the $4^+_1 \to 2^+_1$ transition at 1106.88(2) keV [24] in the γ-ray singles spectra. In these, three contaminant

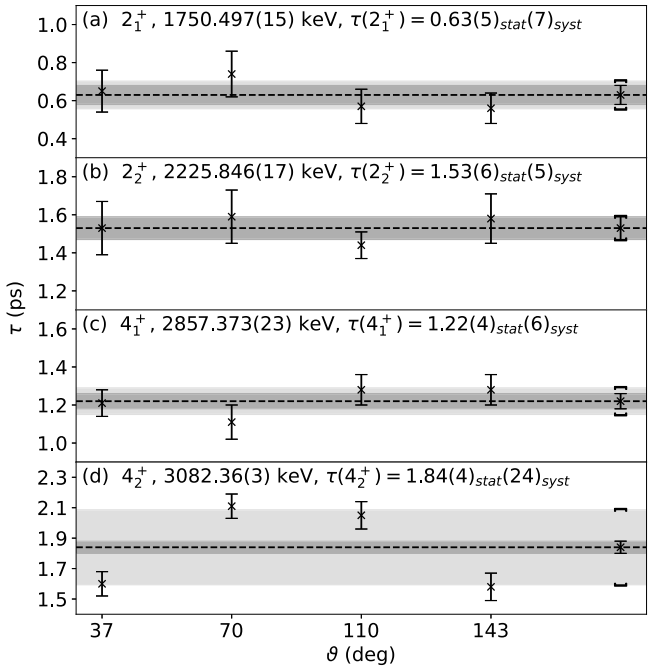


FIG. 5. Lifetimes of the $2^+_{1,2}$ and $4^+_{1,2}$ states determined individually for the ROSPHERE rings at polar angles 37°, 70°, 110°, and 143° (cf. Fig. 4). The systematic uncertainties of the adopted values, indicated by the data points on the right, reflect the spread of results obtained for individual rings.

transitions from ^{94,96}Zr and ^{98}Mo are observed in the energy region of the lineshape [cf. column (c) of Fig. 4]. In forward beam direction, the $7^-_1 \rightarrow 5^-_1$ and $5^-_1 \rightarrow 4^+_1$ transitions of ^{96}Zr and ^{98}Mo at 1114.6 [24] and 1110.77(7) keV [40], respectively, are considered in the lineshape analysis. For their respective parent states, no lifetime information is available in the literature. Since a simultaneous description of the $4^+_1 \rightarrow 2^+_1$ transition's lineshape in all detection angles of ROSPHERE is only achieved for emission of the contaminant γ rays at rest, this assumption is maintained in the ringwise analysis. For detectors placed in backward beam direction, the $3^-_1 \rightarrow 2^+_1$ transition of ^{94}Zr at 1138.88(10) keV [39], which exhibits only a flight component due to its short lifetime of $\tau = 127^{+10}_{-9}$ fs [46], has to be taken into account for a description of the stopped component's high-energy side. Its lifetime, obtained from DSAM following the $(n, n'\gamma)$ reaction [46], is in good agreement with $\tau = 114^{+5}_{-6}$ fs determined in the present work. The combined lineshape analysis of the $4^+_1 \rightarrow 2^+_1$ transition of ^{96}Zr together with the above-mentioned contaminants is shown in column (c) of Fig. 4. The resulting value $\tau(4^+_1) = 1.22(4)_{\text{stat}}(6)_{\text{syst}}$ ps [cf. Fig. 5(c)] is in agreement with $0.86^{+0.67}_{-0.26}$ reported in Ref. [29] but significantly more precise.

For the 4^+_2 state at 3082.36(3) keV [24] a lower limit on the lifetime of 2 ps is reported from DSAM measurements after inelastic neutron scattering [29]. The lineshape analysis based on the dominant decay path to the 3^-_1 state yields an adopted lifetime $\tau(4^+_2) = 1.84(4)_{\text{stat}}(24)_{\text{syst}}$ ps, in agreement with this limit. As evident from Fig. 5(d), spectra from detectors placed at polar angles $\vartheta = 70°$ and 110° yielded lifetimes above 2 ps in contrast to the more extreme forward and backward angles. An appropriate systematic uncertainty is introduced to account for this discrepancy.

Three candidates for 6^+ states at 3309.19(9), 3483.44(9), and 3772.2(4) keV [24] are populated in the present work (cf. Fig. 3). Based on its decay characteristics, a likely (5^+) assignment has recently been proposed for the 3309-keV state [12]. For the state at 3483.44(9) keV [24] a lifetime $\tau(6^+) = 36(13)$ ps is given in the data sheets [24]. The 6^+_3 state at 3772.2(4) keV [24] is depopulated mostly through a 914.85(5)-keV [12] transition to the 4^+_1 state; it is, however, obfuscated by the dominant $2^+_1 \rightarrow 0^+_1$ transition of ^{94}Zr at 918.74(5) keV [39] and, thus, not suitable for a lineshape investigation.

For γ-ray transitions of the $0^+_{3,4}$ states at 2695.18(3) and 2925.55(3) keV [24], respectively, no lineshape is observed, suggesting that they predominantly decay at rest. Since no feeding transitions are observed, it can be concluded that their lifetimes exceed 10 ps in agreement with literature values of 40(10) and 29(20) ps [24].

Of the negative-parity band on top of the 3^-_1 state at 1897.158(16) keV, also the 5^-_1 and 7^-_1 members at 3119.87(3) and 4234.7(5) keV [24], respectively, are populated. While statistics do not suffice for a reliable lifetime analysis of the latter state, no lineshape is visible for the 5^-_1 state despite its reported short lifetime of $\tau(5^-_1) = 840^{+980}_{-300}$ fs [29].

III. DISCUSSION

The new lifetime measurements of the 2^+_2 and $4^+_{1,2}$ states allow for more detailed insights into the nature of the intruder structure of ^{96}Zr built on top of the 0^+_2 state at 1581.64(6) keV [24]. The transition strengths collected in Table I confirm its assumed collectivity and firmly assign the 2^+_2 and 4^+_1 states at 2225.846(17) and 2857.373(23) keV [24], respectively, to it. For the 4^+_1 state at 2857.373(23) keV, transition strengths $B(E2; 4^+_1 \rightarrow 2^+_1) = 11.2(8)$ W.u. and $B(E2; 4^+_1 \rightarrow 2^+_2) = 39(7)$ W.u. are found experimentally (cf. Table I), hinting at mixing with the normal structure; likely through the energetically close-lying 4^+_2 state at 3082.36(3) keV [24] and $B(M1; 4^+_2 \rightarrow 4^+_1) = 0.20(3)\,\mu_N^2$. The experimentally obtained $B(E2; 4^+_2 \rightarrow 2^+_1)$ and $B(E2; 4^+_2 \rightarrow 2^+_2)$ transition strengths, amounting to 0.30(5) and 1.7(4) W.u., respectively, support the assignment of the 4^+_2 state to the normal structure, contrary to the placement in Ref. [12]. The potentially collective nature of the $E2$ transition from the 6^+ state at 3772.2(4) keV [24] to the 4^+_1 state has yet to be proven to affiliate it with the intruder structure. Notably, in Ref. [12] it has, together with the 4^+_1 state, been placed as part of the ground-state structure.

Based on the available data from the 0^+_2, 2^+_2, and 4^+_1 states, the fingerprint quantities $R_{4/2} = [E(4^+_1) - E(0^+_2)]/[E(2^+_2) - E(0^+_2)] = 1.98$ and $B_{4/2} = B(E2; 4^+_1 \rightarrow 2^+_2)/B(E2; 2^+_2 \rightarrow 0^+_2) = 1.5(3)$ are obtained; the latter with greatly improved uncertainties due to the new lifetimes obtained in the present work. In the collective picture, the almost equidistant energy steps between the 0^+_2, 2^+_2, and 4^+_1 states favor a classification as a spherical vibrator. The $B_{4/2}$ value, on the other hand, is

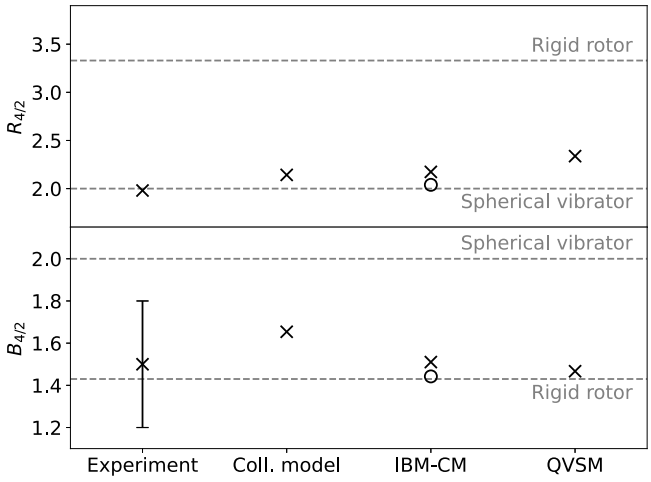


FIG. 6. Comparison of the $R_{4/2}$ and $B_{4/2}$ signatures of the intruder structure of ^{96}Zr to predictions from the collective model [44], the interacting boson model with configuration mixing [21,22] (IBM-CM), and the quasiparticle vacua shell model (QVSM). The circles represent $R_{4/2}$ and $B_{4/2}$ values obtained from IBM-CM calculations with the mixing parameter increased to $\omega = 0.04$ MeV.

located close to $10/7 \approx 1.43$ expected for an idealized rigid rotor [51]. However, also $B_{4/2} = 2$ signifying a spherical vibrator [52] lies within two standard deviations.

In the past, the structure of ^{96}Zr has been discussed in the context of the collective quadrupole model using the Bohr Hamiltonian with [44] and without [53] inclusion of the γ degree of freedom. In both cases, the potential in β features spherical and deformed minima separated by a barrier with the exact characteristics phenomenologically tailored to the known experimental data of low-lying states of ^{96}Zr. With the deformed minimum fixed at $\beta = 0.24$ through the experimental $B(E2; 2_2^+ \to 0_2^+)$ value, the collectivity of the intruder structure is reproduced; in Fig. 6 the calculated $R_{4/2}$ and $B_{4/2}$ values are confronted with their experimental counterparts. By virtue of the constructed potential barrier, the wave functions of the 2_1^+ and 4_1^+ states, while mostly confined to the spherical and deformed minima, respectively, have enough overlap to allow for a collective transition connecting them.

While the description in the collective model presented in Refs. [44,53] is limited to ^{96}Zr, theoretical approaches with the IBM-CM and QVSM offer the opportunity to study the evolution of nuclear structure in the zirconium isotopic chain with increasing neutron number in a consistent framework.

The calculations of the zirconium isotopes in the interacting boson model with configuration mixing [18,19] (IBM-CM) feature valence neutrons above a ^{90}Zr core and two configurations [21–23]. The wave function of an eigenstate with angular momentum L is a linear combination of wave functions corresponding to two configurations A and B with boson numbers $(N, N+2) = (3, 5)$ for ^{96}Zr. The $[N]$- and $[N+2]$-boson spaces, whose size is calculated with respect to the ^{90}Zr core, mimic no active protons above $Z = 40$ and proton $2p$-$2h$ states crossing this subshell gap, respectively. Consequently, a wave function can be written as

$$|\Psi; L\rangle = a\,|\psi_A; [N], L\rangle + b\,|\psi_B; [N+2], L\rangle$$

with $a^2 + b^2 = 1$ and $\psi_{A,B}$ summarizing additional quantum numbers for the sake of readability.

A comparison of the IBM-CM predictions to the experimental results is depicted in Fig. 7, highlighting the overall good reproduction of the low-energy structure of ^{96}Zr. The calculations show a clear separation of the states into two groups, corresponding to normal (configuration A, $[N]$) and intruder (configuration B, $[N+2]$) nature. In agreement with experimental findings [6], a small mixing parameter $\omega = 0.02$ MeV is used in the IBM-CM calculation [21], leading to $0_{1,2}^+$ and $2_{1,2}^+$ states with virtually no mixing as illustrated by wave-function purities of 99.6% and 94.3%, respectively. Similarly to the $M1$ transition between the lowest 2^+ states of each configuration, the underestimated $B(E2; 4_1^+ \to 2_1^+)$ transition strength might, however, hint at the necessity for larger mixing between both structures. In order to probe this, the IBM-CM calculations have been repeated with an increased mixing parameter $\omega = 0.04$ MeV. The choice for the value $\omega = 0.02$ MeV was taken along the $^{96-110}$Zr chain for simplicity, with emphasis on the ^{100}Zr isotope near the critical point of the quantum phase transition [23]. However, a larger value was forced for $^{92-94}$Zr, potentially suggesting the same need for ^{96}Zr, where neutrons mainly occupy the $d_{5/2}$ orbit. As a result, the key $B(M1; 2_2^+ \to 2_1^+)$ and $B(E2; 4_1^+ \to 2_1^+)$ transition strengths are increased to $0.058\,\mu_N^2$ and 8.57 W.u., significantly narrowing the gap to the experimental values of $0.098(6)\,\mu_N^2$ and 11.2(8) W.u., respectively. The effect on the remaining $E2$ transition strengths, which are summarized in Table I, is mild or even beneficial. The wave-function purity remains high for the 0^+ states but drops to 84.7% for the $2_{1,2}^+$ states. As for the calculated intruder 4_1^+ and 6_1^+ states, the mixing remains weak, contrary to the $2_{1,2}^+$ states. This mixing analysis is supported by that of the odd-mass Zr isotopes as well [54], and follows the MCSM work [6], which suggests neutrons mainly occupy the $d_{5/2}$ orbit and weak mixing with the $g_{9/2}$ proton configuration.

Irrespective of the chosen mixing parameter, the IBM-CM predicts a quasispherical, U(5)-like intruder band built on the 0_2^+ state and correctly reproduces its collectivity [cf. Fig. 6(b) and Fig. 7(b)], whereas it tends to overestimate it in neighboring, heavier ^{98}Zr [11].

For a fully microscopic interpretation of the low-energy structure of ^{96}Zr, large-scale quasiparticle vacua shell-model [26,27] (QVSM) calculations have been performed. The QVSM is the most advanced version of the MCSM. In particular, it is more effective for heavier mass regions [26]. The calculations employ the same model space as the ones using the MCSM presented in Ref. [6]; namely for protons the $2p_{3/2}$, $1f_{5/2}$, and $2p_{1/2}$ orbitals as well as the full sdg shell and for neutrons the sdg shell furthermore including the $1h_{11/2}$, $2f_{7/2}$, and $3p_{3/2}$ orbitals above. The employed effective interaction has been modified slightly with respect to the previous MCSM calculations; the changes are, however, relatively minor and the mechanism of shape transition remains essentially unchanged. On the other hand, the description of various properties has been improved. This results in differing occupation numbers, summarized in Fig. 8, for

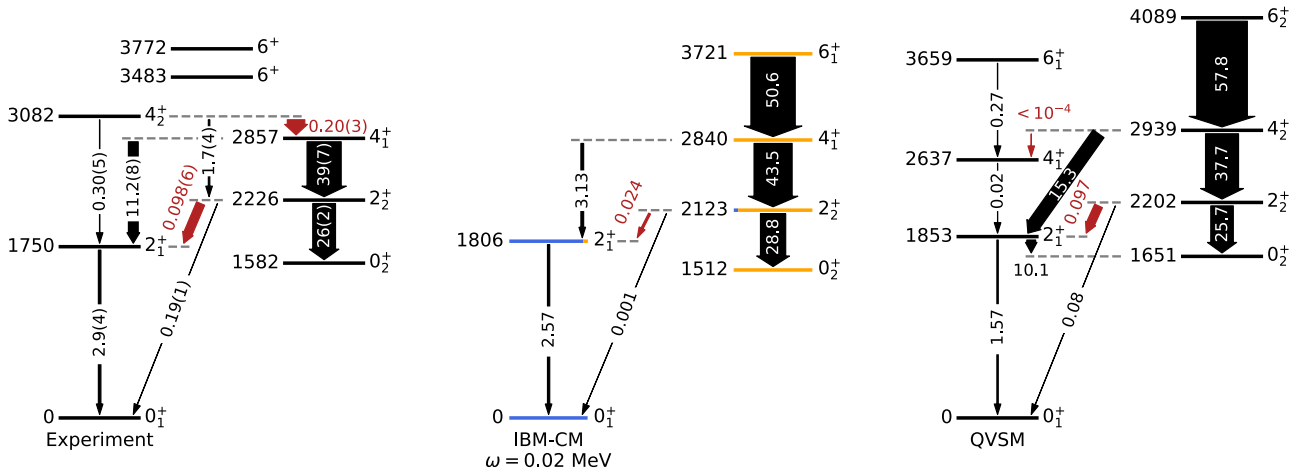


FIG. 7. Comparison of the experimental level scheme with predictions from IBM-CM and QVSM. Excitation energies are given in keV and the strengths of $M1$ and $E2$ transitions in μ_N^2 and W.u., respectively. The thickness of the arrows, which are shown in red and black for $M1$ and $E2$ transitions, respectively, scale with the transition strength. The lines marking states obtained from the IBM-CM calculations are color coded by the fractions of $[N = 3]$ (blue) and $[N = 5]$ (orange) configurations in their wave functions.

some orbitals when compared to the MCSM calculations [6]. In the latter, the ground state of ^{96}Zr is characterized by filled proton and neutron orbitals below the $Z = 40$ and $N = 56$ (sub)shell closures, respectively, whereas those above remain mostly empty. In the QVSM, on the other hand, especially the proton $1g_{9/2}$ and neutron $1h_{11/2}$ orbitals contain, already in the ground state, around one and two nucleons, respectively.

The normal 2^+ and 4^+ states are dominated by single-neutron excitations from the $2d_{5/2}$ orbital; for the former to the $3s_{1/2}$ and for the latter to the $1h_{11/2}$. The deformed 0_2^+ state has in the past been proposed to be of $4p$-$4h$ nature [55,56] with pairs of protons and neutrons promoted across the $Z = 40$ and $N = 56$ (sub)shell closures, respectively. In the present QVSM calculations, on average about one proton is promoted from the $2p_{1/2}$ to the $1g_{9/2}$ orbital and two neutrons are excited from the $2d_{5/2}$ to the $2d_{3/2}$ and $1h_{11/2}$ orbitals. This is in marked contrast to the MCSM results, which suggested that the 0_2^+ and 2_2^+ states contain approximately three proton and three neutron particle-hole excitations on average [5,6]. As a result, their mixing with the spherical $0p$-$0h$ configuration was hindered because two-body interactions cannot directly couple these configurations. The difference in populations implies that near-oblate configurations mix more readily with spherical configurations. Moreover, the type-II shell evolution still plays an important role.

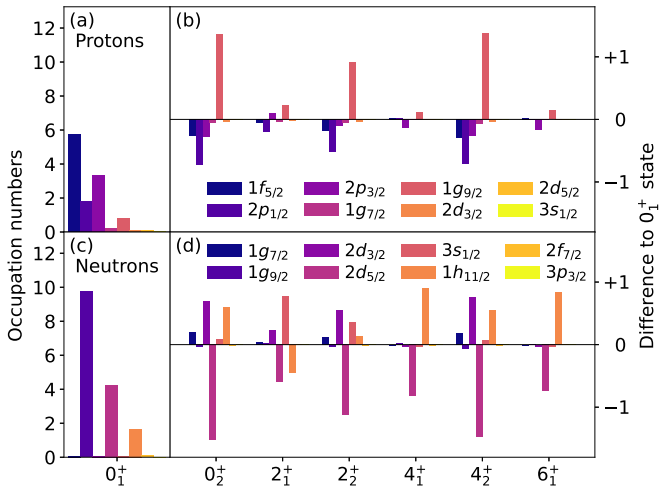


FIG. 8. Occupation numbers of orbitals considered in the QVSM calculations. (a) and (c) depict the proton and neutron occupancies found for the ground state, respectively. The change in occupation numbers for the excited states relative to the 0_1^+ state is shown in (b) and (d). The 4_2^+ state in the QVSM calculations corresponds to the experimentally observed 4_1^+ state and vice versa.

The QVSM calculations agree with the low-lying level scheme of ^{96}Zr as evident from Fig. 7. They furthermore reproduce its hallmark octupole collectivity, predicting the 1897.158(16)-keV [24] 3_1^- state at 1383 keV with $B(E3; 3_1^- \to 0_1^+) = 52.9$ W.u., in agreement with the adopted value of 57(4) W.u. [24] and within 20% of 42(3) W.u. reported in Ref. [10]. However, the calculations do not replicate the almost equidistant excitation energies within the excited-state structure shown in Fig. 6. While the ordering of the 0^+ and 2^+ states is correct, the calculations do not reproduce the relative ordering of the $4_{1,2}^+$ states as inferred from their experimentally determined $E2$ transition strengths (cf. Table I); contrasting the evolution of relative excitation energies between collective and noncollective states with neutron number toward the shape-phase transition [57]. In the following, the first (second) 4^+ state from the QVSM calculations is associated with the 4_2^+ (4_1^+) state observed at 3082.36(3) keV [2857.373(23) keV] [24].

The nature of the calculated states can be inferred from the T plots [4] shown in Fig. 9, which visualize the importance of QVSM basis states in a potential-energy surface spanned by the quadrupole moments Q_{20} and Q_{22}. The 0^+ states show little mixing, in agreement with the conclusions of Ref. [6]. In contrast, the 2^+ states, which are predicted at 1853 and 2202 keV, are more strongly mixed as evident from the sizeable contributions of deformed (spherical) basis states

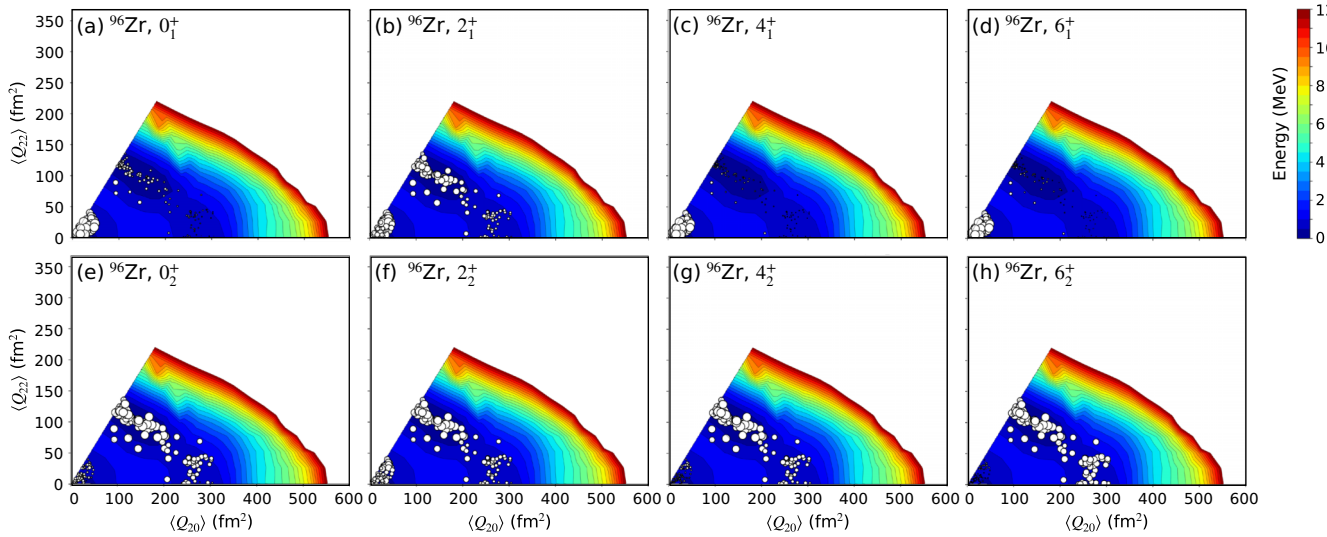


FIG. 9. T plots for the $0^+_{1,2}$, $2^+_{1,2}$, $4^+_{1,2}$, and $6^+_{1,2}$ states of ^{96}Zr from the QVSM calculations. The top and bottom rows contain states associated with the (spherical) normal and (triaxially deformed) intruder structures, respectively. The circles mark the locations of basis vectors present in the QVSM eigenstate corresponding to the state in a potential-energy surface spanned by quadrupole moments Q_{20} and Q_{22}. The area of the circle encodes the importance of a basis vector in the eigenstate. The T plots for the 2^+ states reveal the existence of sizeable mixing. The deformed 4^+_2 state from the QVSM calculations corresponds to the 4^+_1 state in the experimental level scheme of ^{96}Zr and vice versa.

to the wave function of the 2^+_1 (2^+_2) state. For the 4^+ and 6^+ states the situation is again similar to the one found for the 0^+ states, showing a clear separation between spherical and triaxially deformed configurations. Compared to the MCSM calculations, the potential appears somewhat softer in the γ degree of freedom as inferred from the larger spread of the basis-state markers (cf. Figs. 9 and 3 of Ref. [6]).

The predicted $E2$ transition strengths are in close agreement with the experimental results (cf. Table I and Fig. 7). The more developed mixing found for the 2^+ states is likely one of the reasons for the reproduction of the collective $B(M1; 2^+_2 \to 2^+_1)$ and $B(E2; 4^+_1 \to 2^+_1)$ interband transitions, which were underestimated in the previous MCSM calculations. The large $B(M1; 4^+_2 \to 4^+_1) = 0.20(3)\,\mu_N^2$ transition strength is, however, greatly underestimated; even when correcting for the smaller transition energy in the experimental data (cf. Fig. 7). In a simplified picture, this might indicate the necessity for more strongly mixed 4^+ states in the QVSM.

In order to probe the wave-function composition of the observed states from the experimental perspective, a two-state model (TSM) analysis based on the $E2$ transition rates collected in Table I is appropriate. The observed states $|J^+_1\rangle$ and $|J^+_2\rangle$ are treated as linear combinations of basis states $|J^+_\mathrm{I}\rangle$ and $|J^+_\mathrm{II}\rangle$, which correspond to normal (spherical) and intruder (deformed) configurations I and II, respectively, yielding

$$\begin{pmatrix} |J^+_1\rangle \\ |J^+_2\rangle \end{pmatrix} = \begin{pmatrix} \alpha_J & \beta_J \\ -\beta_J & \alpha_J \end{pmatrix} \begin{pmatrix} |J^+_\mathrm{I}\rangle \\ |J^+_\mathrm{II}\rangle \end{pmatrix}$$

with the identities $\alpha_J^2 + \beta_J^2 = 1$ and $J \in \{0, 2, 4\}$. All interband $E2$ matrix elements between the pure configurations I and II are assumed to vanish. Following the ansatz of Fortune [58], dimensionless ratios of mixing parameters β_J/α_J and $E2$ matrix elements calculated from the transition strengths found in Table I are used. The phases of the $2^+_1 \to 0^+_1$ and $2^+_2 \to 0^+_1$ matrix elements are required to be positive, whereas all others can also be negative. If the TSM is limited to the $0^+_{1,2}$ and $2^+_{1,2}$ states, i.e., to the situation discussed in Ref. [58], wave-function purities of 98.1(3)% and 97.1(4)% are found, respectively. If a negative sign is chosen for the small $2^+_2 \to 0^+_1$ matrix element, in contrast to results from a Coulomb-excitation analysis [25], a second solution with purities 99.9(1)% and 89.5(4)% is obtained. In both cases, the ratio between intrinsic matrix elements in the normal (configuration I) and intruder (configuration II) structures, $r^{20} = \langle 2^+_\mathrm{I}\|T(E2)\|0^+_\mathrm{I}\rangle / \langle 2^+_\mathrm{II}\|T(E2)\|0^+_\mathrm{II}\rangle$, is around 0.3, implying collectivity in structure II. For the hitherto unobserved $2^+_1 \to 0^+_2$ transition, $E2$ strengths of 0.41(6) and 2.9(2) W.u. are predicted by the TSM, again contingent on the sign of the $2^+_2 \to 0^+_1$ matrix element.

The situation changes considerably when the newly obtained transitions from the $4^+_{1,2}$ states (cf. Table I) are incorporated. Notably, the 2^+ states are now also influenced by the collective $4^+_1 \to 2^+_1$ transition with $B(E2; 4^+_1 \to 2^+_1) = 11.2(8)$ W.u. (cf. Table I). The ratio of intrinsic matrix elements between the 4^+ and 2^+ states, r^{42}, is defined analogous to the aforementioned r^{20}. The resulting system comprises five matrix elements with free phases; namely from the $2^+_2 \to 0^+_1$ and all transitions between the 4^+ and 2^+ states. In the following, only those sign combinations resulting in a close reproduction of the experimental matrix elements are considered. Exemplarily, the results for all positive phases are collected in Table II. Irrespective of the chosen signs, the 0^+ and 4^+ states show little mixing, whereas the wave-function purities of the 2^+ states drop to around 80%, comparable to the IBM-CM calculations with increased mixing. The encountered scenario resembles the situation found in the QVSM calculations, visualized in the T plots of Fig. 9. In these, the 4^+ (and 6^+) states appear slightly less mixed

TABLE II. Parameters for exemplary TSM analyses, when limited to the $(0^+, 2^+)$ states and for inclusion of the 4^+ states. In the latter case, the reproduction of experimental results deteriorates considerably if equal ratios of intrinsic matrix elements r^{20} and r^{42} are required. The last two lines state the degree-of-freedom ν of the considered system and the obtained goodness-of-fit χ^2_ν. The calculations assumed positive phases for all matrix elements.

J	Parameter	$(0^+, 2^+)$	$(0^+, 2^+, 4^+)$	
			$r^{20} \neq r^{42}$	$r^{20} = r^{42}$
0	α_0^2	0.981(3)	0.959(5)	0.981(4)
	β_0^2	0.019(3)	0.041(5)	0.019(4)
	$V_{\rm mix}$ (keV)	217(14)	311(20)	217(21)
2	α_2^2	0.971(4)	0.81(3)	0.67(8)
	β_2^2	0.029(4)	0.19(3)	0.33(8)
	$V_{\rm mix}$ (keV)	79(4)	186(11)	220(19)
4	α_4^2		0.969(6)	0.990(6)
	β_4^2		0.031(6)	0.010(6)
	$V_{\rm mix}$ (keV)		38(3)	21(6)
	r^{20}	0.31(3)	0.24(3)	0.10(1)
	r^{42}		0.001(3)	0.10(1)
	ν	0	2	3
	χ^2_ν	0.0	2.8	83.7

than the 0^+ states. The fact that the TSM results of Table II support this observation might, however, be fortuitous. The transition strength $B(E2; 2_1^+ \rightarrow 0_2^+) = 10.1$ W.u. predicted in the QVSM is twice as large as 5(1) W.u. obtained from the full TSM based on the experimental transition strengths of Table I. Notably, the latter value is, in turn, about 70% larger than from the TSM limited to the $(0^+, 2^+)$ states by virtue of the increased mixing in the 2^+ states.

The TSM shows that the necessity for considerably mixed 2^+ states can be concluded already from the experimental data under relatively weak assumptions, in close agreement with the predicted structure of the wave functions of both the IBM-CM and QVSM.

IV. SUMMARY

In summary, excited states of ^{96}Zr, populated in the ^{94}Zr(^{18}O, ^{16}O)^{96}Zr two-neutron transfer reaction, have been studied with the Doppler-shift attenuation method. The measured lifetimes firmly attribute the 2_2^+ and 4_1^+ states at 2225.846(17) and 2857.373(23) keV [24], respectively, to the intruder structure on top of the 1581.64(6)-keV [24] 0_2^+ state. Calculations in the algebraic interacting boson model with configuration mixing and the quasiparticle vacua shell model are able to successfully reproduce the transition strengths and both offer interpretations of coexisting normal and intruder configurations, with some difference in the shape of the intruder configuration. Comparison to a simple two-state mixing model highlights the importance of sizeable mixing in the 2^+ states for a reproduction of the observed $E2$ transition strengths. A collective $4_2^+ \rightarrow 4_1^+$ interband $M1$ transition might hint at non-negligible mixing between the normal and intruder structures also at $J = 4$.

The present work shows that further data are needed to understand the nature of the excited states of ^{96}Zr. The QVSM predicts quadrupole moments of 29.3 $e$fm^2 and 43.7 $e$fm^2 for the 2_1^+ and 2_2^+ states and 59.3 $e$fm^2 and -2.71 $e$fm^2 for the 4_1^+ and 4_2^+ states, respectively, reflecting the enhanced mixing found for the 2^+ states (cf. Fig. 9). In contrast, the quadrupole moments put forward by the IBM-CM calculations (for $\omega = 0.02$ MeV) are 5.8 $e$fm^2, 21.9 $e$fm^2, and 37.1 $e$fm^2 for the 2_1^+, 2_2^+, and 4_1^+ states, respectively, reflecting their more spherical character. The small excitation strengths from the ground state to both 2^+ states might, however, make a determination of their quadrupole moments via safe Coulomb excitation [59] prohibitively complicated. A measurement of the 2^+ states' (relative) population probability, for instance in the ^{94}Zr$(t, p)^{96}$Zr reaction, might be used instead to probe the wave-function overlaps between the $2_{1,2}^+$ states of ^{96}Zr and the ground state of ^{94}Zr [60] and, thus, reveal structural differences between the final states of ^{96}Zr. In the literature, however, only cross sections for two-neutron transfer to the ground and excited 0^+ states of ^{96}Zr are available to date [24,61].

ACKNOWLEDGMENTS

The authors thank the staff of the IFIN-HH tandem accelerator for providing excellent experimental conditions. Support by R. Kern and W. Witt during data taking is gratefully acknowledged. T.B. and T.S. are indebted to C. Stahl for initial help with the APCAD program. This work was supported by the BMBF under Grants No. 05P18RDEN9 and No. 05P18RDFN1/9, by the Deutsche Forschungsgemeinschaft (DFG, German Research Foundation) under Project-ID 499256822 – GRK 2891 "Nuclear Photonics," and by the Institute of Atomic Physics, Romania, under Project ELI-RO/DFG/2023_001 ARNPhot. K.Y. was supported by MEXT as "Program for Promoting Researches on the Supercomputer Fugaku" (JPMXP1020200105 and JPMXP1020230411), the JSPS KAKENHI under Grants No. JP22K14031 and No. JP25K17404, as well as the general use program in CCS, University of Tsukuba. K.Y. used computational resources of the supercomputer Fugaku provided by the RIKEN Center for Computational Science (Project IDs hp230137 and hp250187) and the supercomputer Pegasus provided by CCS, University of Tsukuba. This project has received funding from the European Union's Horizon 2020 research and innovation programme under Grant Agreement No. 654002 (ENSAR-2) and the Romanian National Authority for Research through the Nucleu Project No. PN 23 21 01 02.

DATA AVAILABILITY

The data that support the findings of this article are not publicly available upon publication because it is not technically feasible and/or the cost of preparing, depositing, and hosting the data would be prohibitive within the terms of this research project. The data are available from the authors upon reasonable request.

[1] P. Federman and S. Pittel, Unified shell-model description of nuclear deformation, Phys. Rev. C **20**, 820 (1979).

[2] T. Otsuka, T. Suzuki, R. Fujimoto, H. Grawe, and Y. Akaishi, Evolution of nuclear shells due to the tensor force, Phys. Rev. Lett. **95**, 232502 (2005).

[3] T. Otsuka, T. Suzuki, M. Honma, Y. Utsuno, N. Tsunoda, K. Tsukiyama, and M. Hjorth-Jensen, Novel features of nuclear forces and shell evolution in exotic nuclei, Phys. Rev. Lett. **104**, 012501 (2010).

[4] T. Otsuka and Y. Tsunoda, The role of shell evolution in shape coexistence, J. Phys. G: Nucl. Part. Phys. **43**, 024009 (2016).

[5] T. Togashi, Y. Tsunoda, T. Otsuka, and N. Shimizu, Quantum phase transition in the shape of Zr isotopes, Phys. Rev. Lett. **117**, 172502 (2016).

[6] C. Kremer, S. Aslanidou, S. Bassauer, M. Hilcker, A. Krugmann, P. von Neumann-Cosel, T. Otsuka, N. Pietralla, V. Y. Ponomarev, N. Shimizu, M. Singer, G. Steinhilber, T. Togashi, Y. Tsunoda, V. Werner, and M. Zweidinger, First measurement of collectivity of coexisting shapes based on type II shell evolution: The case of ^{96}Zr, Phys. Rev. Lett. **117**, 172503 (2016).

[7] S. Ansari, J.-M. Régis, J. Jolie, N. Saed-Samii, N. Warr, W. Korten, M. Zielińska, M.-D. Salsac, A. Blanc, M. Jentschel, U. Köster, P. Mutti, T. Soldner, G. S. Simpson, F. Drouet, A. Vancraeyenest, G. de France, E. Clément, O. Stezowski, C. A. Ur, *et al.*, Experimental study of the lifetime and phase transition in neutron-rich ^{98,100,102}Zr, Phys. Rev. C **96**, 054323 (2017).

[8] W. Witt, V. Werner, N. Pietralla, M. Albers, A. D. Ayangeakaa, B. Bucher, M. P. Carpenter, D. Cline, H. M. David, A. Hayes, C. Hoffman, R. V. F. Janssens, B. P. Kay, F. G. Kondev, W. Korten, T. Lauritsen, O. Möller, G. Rainovski, G. Savard, D. Seweryniak, *et al.*, Sub-shell closure and shape coexistence in the transitional nucleus ^{98}Zr, Phys. Rev. C **98**, 041302 (2018).

[9] P. Singh, W. Korten, T.W. Hagen, A. Görgen, L. Grente, M.-D. Salsac, F. Farget, E. Clément, G. de France, T. Braunroth, B. Bruyneel, I. Celikovic, O. Delaune, A. Dewald, A. Dijon, J.-P. Delaroche, M. Girod, M. Hackstein, B. Jacquot, J. Libert, *et al.*, Evidence for coexisting shapes through lifetime measurements in ^{98}Zr, Phys. Rev. Lett. **121**, 192501 (2018).

[10] Ł. W. Iskra, R. Broda, R. V. F. Janssens, M. P. Carpenter, B. Fornal, T. Lauritsen, T. Otsuka, T. Togashi, Y. Tsunoda, W. B. Walters, and S. Zhu, Revised B(E3) transition rate and structure of the 3^- level in ^{96}Zr, Phys. Lett. B **788**, 396 (2019).

[11] V. Karayonchev, J. Jolie, A. Blazhev, A. Dewald, A. Esmaylzadeh, C. Fransen, G. Häfner, L. Knafla, J. Litzinger, C. Müller-Gatermann, J.-M. Régis, K. Schomacker, A. Vogt, N. Warr, A. Leviatan, and N. Gavrielov, Tests of collectivity in ^{98}Zr by absolute transition rates, Phys. Rev. C **102**, 064314 (2020).

[12] J. Wiśniewski, W. Urban, T. Rząca-Urban, K. Sieja, A. Blanc, M. Jentschel, C. Micheagnoli, P. Mutti, U. Köster, G. de France, G. S. Simpson, and C. A. Ur, Structure of $N = 56$ isotones with $36 \leqslant Z \leqslant 42$ protons, Phys. Rev. C **108**, 024302 (2023).

[13] A. Pfeil, K. Nomura, N. Gavrielov, J.-M. Régis, U. Köster, Y. H. Kim, A. Esmaylzadeh, A. Harter, J. Jolie, L. Knafla, M. Ley, and V. Karayonchev, Lifetime measurements in ^{99}Nb and ^{99}Zr: Investigation of shape coexistence, Phys. Rev. C **108**, 034310 (2023).

[14] J. Wu, M. P. Carpenter, F. G. Kondev, R. V. F. Janssens, S. Zhu, E. A. McCutchan, A. D. Ayangeakaa, J. Chen, J. Clark, D. J. Hartley, T. Lauritsen, N. Pietralla, G. Savard, D. Seweryniak, and V. Werner, Determination of the spins and parities for the 0_4^+ and 0_5^+ states in ^{100}Zr, Phys. Rev. C **109**, 024314 (2024).

[15] A. Petrovici, Triple shape coexistence and shape evolution in the $N = 58$ Sr and Zr isotopes, Phys. Rev. C **85**, 034337 (2012).

[16] T. Otsuka, M. Honma, T. Mizusaki, N. Shimizu, and Y. Utsuno, Monte Carlo shell model for atomic nuclei, Prog. Part. Nucl. Phys. **47**, 319 (2001).

[17] N. Shimizu, T. Abe, Y. Tsunoda, Y. Utsuno, T. Yoshida, T. Mizusaki, M. Honma, and T. Otsuka, New-generation Monte Carlo shell model for the K computer era, Prog. Theo. Exp. Phys. **2012**, 01A205 (2012).

[18] P. D. Duval and B. R. Barrett, Configuration mixing in the interacting boson model, Phys. Lett. B **100**, 223 (1981).

[19] P. D. Duval and B. R. Barrett, Quantitative description of configuration mixing in the interacting boson model, Nucl. Phys. A **376**, 213 (1982).

[20] J. E. García-Ramos and K. Heyde, Quest of shape coexistence in Zr isotopes, Phys. Rev. C **100**, 044315 (2019).

[21] N. Gavrielov, A. Leviatan, and F. Iachello, Intertwined quantum phase transitions in the Zr isotopes, Phys. Rev. C **99**, 064324 (2019).

[22] N. Gavrielov, A. Leviatan, and F. Iachello, Interplay between shape-phase transitions and shape coexistence in the Zr isotopes, Phys. Scr. **95**, 024001 (2020).

[23] N. Gavrielov, A. Leviatan, and F. Iachello, Zr isotopes as a region of intertwined quantum phase transitions, Phys. Rev. C **105**, 014305 (2022).

[24] D. Abriola and A. Sonzogni, Nuclear data sheets for A = 96, Nucl. Data Sheets **109**, 2501 (2008).

[25] M. Zielińska, P.E. Garrett, M. Rocchini, S. Pannu, A. Bergmaier, V. Bildstein, A.B. Calder, S.R. Dworatzek, V. Vedia, Z.T. Ahmed, C. Andreoiu, D.W. Annen, H. Asch, A.A. Avaa, G.C. Ball, S. Buck, R.J. Coleman, A. Diaz Varela, D.T. Doherty, J.T.H. Dowie, *et al.*, Collectivity of the deformed structure in ^{96}Zr from complementary Coulomb-excitation and β-decay measurements, Phys. Lett. B **877**, 140481 (2026).

[26] N. Shimizu, Y. Tsunoda, Y. Utsuno, and T. Otsuka, Variational approach with the superposition of the symmetry-restored quasiparticle vacua for nuclear shell-model calculations, Phys. Rev. C **103**, 014312 (2021).

[27] N. Shimizu, K. Yanase, Y. Tsunoda, and T. Otsuka, Monte Carlo shell model and quasi-particle vacua shell model for massively parallel computation, J. Subat. Part. Cosmol. **4**, 100188 (2025).

[28] W. Witt, N. Pietralla, V. Werner, and T. Beck, Data on the structural coexistence in the ^{96}Zr nucleus, Eur. Phys. J. A **55**, 79 (2019).

[29] T. Belgya, G. Molnár, B. Fazekas, Á. Verbs, R. A. Gatenby, and S. W. Yates, Doppler-shift lifetime measurements in ^{96}Zr with the inelastic neutron scattering reaction, Nucl. Phys. A **500**, 77 (1989).

[30] S. Dobrescu, D. V. Mosu, D. Moisa, and S. Papureanu, The Bucharest FN tandem accelerator: Modernization and development, AIP Conf. Proc. **1099**, 51 (2009).

[31] T. K. Alexander and J. S. Forster, Lifetime measurements of excited nuclear levels by Doppler-shift methods, in *Advances in Nuclear Physics: Volume 10*, edited by M. Baranger and E. Vogt (Springer US, Boston, 1978), p. 197.

[32] P. J. Nolan and J. F. Sharpey-Schafer, The measurement of the lifetimes of excited nuclear states, Rep. Prog. Phys. **42**, 1 (1979).

[33] T. Beck, C. Costache, R. Lică, N. Mărginean, C. Mihai, R. E. Mihai, O. Papst, S. Pascu, N. Pietralla, C. Sotty, L. Stan, A. E. Turturică, V. Werner, J. Wiederhold, and W. Witt, SORCERER: A novel particle-detection system for transfer-reaction experiments at ROSPHERE, Nucl. Instrum. Meth. Phys. Res. A **951**, 163090 (2020).

[34] https://github.com/TB-IKP/SORCERER.

[35] D. Bucurescu, I. Căta-Danil, G. Ciocan, C. Costache, D. Deleanu, R. Dima, D. Filipescu, N. Florea, D.G. Ghiţă, T. Glodariu, M. Ivaşcu, R. Lică, N. Mărginean, R. Mărginean, C. Mihai, A. Negret, C.R. Niţă, A. Olăcel, S. Pascu, T. Sava, *et al.*, The ROSPHERE γ-ray spectroscopy array, Nucl. Instrum. Meth. Phys. Res. A **837**, 1 (2016).

[36] A. Gavron, Statistical model calculations in heavy ion reactions, Phys. Rev. C **21**, 230 (1980).

[37] O. B. Tarasov and D. Bazin, LISE++: Radioactive beam production with in-flight separators, Nucl. Instrum. Meth. Phys. Res. B **266**, 4657 (2008).

[38] PACE4 with LISE++, http://lise.nscl.msu.edu/pace4.

[39] D. Abriola and A. A. Sonzogni, Nuclear data sheets for A = 94, Nucl. Data Sheets **107**, 2423 (2006).

[40] J. Chen and B. Singh, Nuclear data sheets for A = 98, Nucl. Data Sheets **164**, 1 (2020).

[41] C. Stahl, J. Leske, M. Lettmann, and N. Pietralla, APCAD—Analysis program for the continuous-angle DSAM, Comput. Phys. Commun. **214**, 174 (2017).

[42] J. F. Ziegler, M. D. Ziegler, and J. P. Biersack, SRIM – The stopping and range of ions in matter (2010), Nucl. Instrum. Meth. Phys. Res. B **268**, 1818 (2010).

[43] F. James, CERN program library long writeup d506 (1994), https://cds.cern.ch/record/2296388/files/minuit.pdf.

[44] E. V. Mardyban, E. A. Kolganova, T. M. Shneidman, R. V. Jolos, and N. Pietralla, Description of the low-lying collective states of ^{96}Zr based on the collective Bohr Hamiltonian including the triaxiality degree of freedom, Phys. Rev. C **102**, 034308 (2020).

[45] G. Kumbartzki, N. Benczer-Koller, J. Holden, G. Jakob, T. Mertzimekis, M. Taylor, K.-H. Speidel, R. Ernst, A. Stuchbery, C. Beausang, and R. Krücken, Competition between proton and neutron excitations in ^{96}Zr, Phys. Lett. B **562**, 193 (2003).

[46] E. E. Peters, A. Chakraborty, B. P. Crider, B. H. Davis, M. K. Gnanamani, M. T. McEllistrem, F. M. Prados-Estévez, J. R. Vanhoy, and S. W. Yates, Level lifetimes in the stable Zr nuclei: Effects of chemical properties in Doppler-shift measurements, Phys. Rev. C **88**, 024317 (2013).

[47] H. Mach, S. Ćwiok, W. Nazarewicz, B. Fogelberg, M. Moszyński, J. Winger, and R. L. Gill, Strong octupole and dipole collectivity in ^{96}Zr: Indication for octupole instability in the $A = 100$ mass region, Phys. Rev. C **42**, R811 (1990).

[48] A.M. Van Den Berg, A. Saha, G.D. Jones, L.W. Put, and R.H. Siemssen, Study of even-A zirconium and strontium isotopes with the (d, ^{6}Li) reaction, Nucl. Phys. A **429**, 1 (1984).

[49] E. R. Flynn, D. D. Armstrong, and J. G. Beery, Inelastic triton scattering from ^{92,94,96}Zr, Phys. Rev. C **1**, 703 (1970).

[50] S. K. Basu and E. A. Mccutchan, Nuclear data sheets for A = 90, Nucl. Data Sheets **165**, 1 (2020).

[51] A. Bohr and B. R. Mottelson, Collective and individual-particle aspects of nuclear structure, Mat. Fys. Medd. Dan. Vid. Selsk. **27**, 1 (1953).

[52] G. Scharff-Goldhaber and J. Weneser, System of even-even nuclei, Phys. Rev. **98**, 212 (1955).

[53] D. A. Sazonov, E. A. Kolganova, T. M. Shneidman, R. V. Jolos, N. Pietralla, and W. Witt, Description of shape coexistence in ^{96}Zr based on the quadrupole-collective Bohr Hamiltonian, Phys. Rev. C **99**, 031304 (2019).

[54] N. Gavrielov, Competing shape evolution, crossing configurations, and single particle levels in nuclei, Phys. Rev. Res. **7**, L022022 (2025).

[55] K. Heyde, P. Van Isacker, R.F. Casten, and J.L. Wood, A shell-model interpretation of intruder states and the onset of deformation in even-even nuclei, Phys. Lett. B **155**, 303 (1985).

[56] K. Heyde and J. L. Wood, Shape coexistence in atomic nuclei, Rev. Mod. Phys. **83**, 1467 (2011).

[57] V. Werner, W. Witt, T. Beck, N. Pietralla, M. Boromiza, C. Clisu, C. Costache, I.E. Dinescu, A. Ionescu, P.R. John, P. Koseoglou, N. Margineăn, R. Margineăn, C. Mihai, R.E. Mihai, A. Mitu, A. Negret, C.R. Nita, A. Olacel, S. Pascu, *et al.*, Shape transitions between and within Zr isotopes, EPJ Web Conf. **223**, 01070 (2019).

[58] H. T. Fortune, Shape coexistence and mixing in ^{96}Zr, Phys. Rev. C **95**, 054313 (2017).

[59] D. Cline, Nuclear shapes studied by Coulomb excitation, Annu. Rev. Nucl. Part. Sci. **36**, 683 (1986).

[60] H. T. Fortune, Coexistence and $2n$ transfer in even Zr nuclei, Phys. Rev. C **100**, 034303 (2019).

[61] J. G. Beery, A study of the (t,p) reaction on ^{90,92,94,96}Zr and ^{122,124}Sn, Ph.D. thesis, University of New Mexico, 1969.